Proceedings of the Fifteenth International Conference on
Computational Structures Technology
Edited by: P. Iványi, J. Kruis and B.H.V. Topping
Civil-Comp Conferences, Volume 9, Paper 9.1
Civil-Comp Press, Edinburgh, United Kingdom, 2024
ISSN: 2753-3239, doi: 10.4203/ccc.9.9.1

Automatic Remeshing Procedure for Limit Analysis with Unstructured Triangular Mesh

Y. Hua and G. Milani

Department of Architecture, Built Environment and Construction Engineering, Politecnico di Milano
Italy

Abstract

This paper presents a novel remeshing procedure for limit analysis with a more general mesh configuration. The element with high dissipation in each analysis step will be refined through three schemes. A benchmark study of the strip footing problem is first carried out to compare the effect of these three refinements, through which the best refinement approach is concluded. Then, in the collapse analysis of Prestwood Bridge, this best refinement is employed to remesh the elements in the backfill region to test the robustness of the remeshing procedure in the practical scenario. The results show that the proposed remeshing procedure for the limit analysis can effectively reduce the mesh dependence of the prediction. The load prediction significantly decreases after iterative refinements in the two considered case studies. According to the benchmark study of strip footing, the edge-split approach has a prominently good performance among the three considered refinement, giving a precise final prediction with only 8 – 15% computational budget of the other two methods. The performance of this approach is also fair when applied to analyzing Prestwood Bridge while the explosion of the time consumption probably appears in the later iterations.

Keywords: limit analysis, remeshing, mesh dependence, strip footing, masonry arch bridges, collapse performance.

1 Introduction

Finite element limit analysis is one of the promising numerical approaches to investigate the progressive failure of the continuum. This approach is developed based on

the theoretical framework of limit analysis but absorbs the idea of domain and field discretization from the classic finite element method. Strong discontinuities, such as cracks and sliding, are convenient to take into account in this approach. If the associated flow rule is adopted, the problem can be stated as Linear Programming (LP), solved in a single step rather than the iterative non-linear finite element analysis procedure. Such analysis has been widely implemented for understanding the collapse of many geomechanics problems [1-6] as well as modeling the failure of the soil-like material in structural analyses [7-10], being proven to have great accuracy and efficiency.

Given the usage of discretization, the mesh dependence of the results should be a great concern. However, this aspect is normally excluded in most of the literature. Automatic remeshing procedure is a very suitable approach to reduce the mesh dependence of the results. This approach has been widely used in finite element analysis [11-12] and is also convenient to be migrated for limit analysis. Unfortunately, current mesh refinement procedures for the limit analysis usually have difficulties applying to a more general scenario. In some contributions, the proposed refinement schemes are only compatible with the regular mesh [13-14]. Regarding some adaptive approaches, cautious assignment of the refinement scheme to different domains according to the property of the prior-known analytical solution is required to get a more precise prediction [15-16]. Therefore, a more general and automatic remeshing procedure for limit analysis is necessary to be put forward.

This paper will develop a fully automatic remeshing procedure for the limit analysis, applicable for more random unstructured triangular mesh. The remeshing will be iteratively conducted until reaching the convergence criterion. In each step of this procedure, the triangles with high dissipation will be selected and then refined through three different schemes. We first apply this procedure to analyze the collapse of the strip footing problem as a benchmark to investigate the effect of different refinement schemes. Then, the collapse of Prestwood Bridge with full consideration of the backfill is investigated. We implement this remeshing procedure to refine the element in the backfill region.

2 Methods

2.1 Deformable triangular elements with constant strain

We first briefly review the theoretical construction of the deformable triangular element with a constant strain field, proposed by Sloan and Kleeman in 1995 [4]. The governing formulation of the element is stated from a kinematic view based on the Upper Bound (UB) theorem.

According to the elasticity theory, the velocity field of the continuum with constant strain can be represented by Eq. (1), where the first part accounts for the rigid body motion and the second one indicates the homogenous deformation mode. Note that here in each mapping, the origin of the coordinate is set at the centroid of the element.

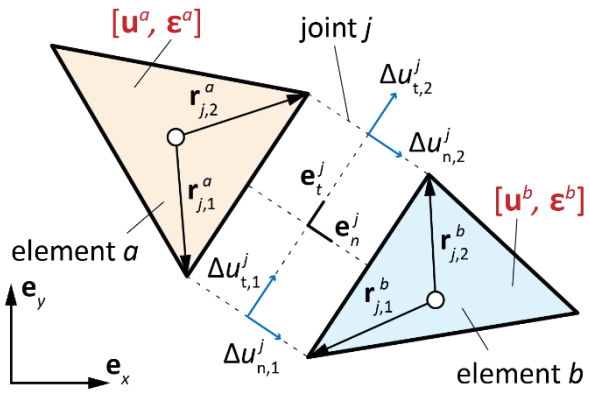

Figure 1: Joint *j* with two adjacent triangular elements *a* and *b*: calculation of velocity discontinuities.

$$\begin{aligned}
&\mathbf{u}^i(x,y) = \mathbf{H}^i_{\mathrm{R}}(x,y)\mathbf{u}^i_{\mathrm{R}} + \mathbf{H}^i_{\mathrm{C}}(x,y)\mathbf{u}^i_{\mathrm{C}} \\
&\mathbf{H}^i_{\mathrm{R}}(x,y) = \begin{bmatrix} 1 & 0 & -y \\ 0 & 1 & x \end{bmatrix},\ \mathbf{u}^i_{\mathrm{R}} := \begin{bmatrix} u^i_x & u^i_y & \omega^i \end{bmatrix}^T \\
&\mathbf{H}^i_{\mathrm{C}}(x,y) = \begin{bmatrix} x & 0 & y \\ 0 & y & x \end{bmatrix},\ \mathbf{u}^i_{\mathrm{C}} := \begin{bmatrix} \varepsilon^i_x & \varepsilon^i_y & \varepsilon^i_{xy} \end{bmatrix}^T
\end{aligned} \tag{1}$$

After clarifying the element velocity field, the velocity discontinuities $\mathbf{q}_j$ at each joint are thus computable. Consider two adjacent triangular elements *a* and *b* with a shared joint *j* (Figure 1), we subtract velocities at the corresponding vertices in elements *a* and *b* and then project such subtraction onto the local frame of the joint (Eq. (2)). A relation between the element unknowns and interfacial velocity jumps can be obtained (Eq. (2)), known as the compatibility condition of limit analysis. Assembling this condition over all the joints, we can write this compatibility constraint in a global matrix form (Eq. (4)).

$$\begin{aligned}
\mathbf{q}_j &= \left[\Delta u^j_{\mathrm{n},1}, \Delta u^j_{\mathrm{t},1}, \Delta u^j_{\mathrm{n},2}, \Delta u^j_{\mathrm{t},2}\right]^T = \begin{bmatrix} \mathbf{Q}_j\mathbf{u}^b(\mathbf{r}^b_1) - \mathbf{Q}_j\mathbf{u}^a(\mathbf{r}^a_1) \\ \mathbf{Q}_j\mathbf{u}^b(\mathbf{r}^b_2) - \mathbf{Q}_j\mathbf{u}^a(\mathbf{r}^a_2) \end{bmatrix} \\
&= \begin{bmatrix} -\left(\mathbf{A}^a_{j,u}\right)^T & \left(\mathbf{A}^b_{j,u}\right)^T \end{bmatrix} \begin{bmatrix} \mathbf{u}^a \\ \mathbf{u}^b \end{bmatrix} + \begin{bmatrix} -\left(\mathbf{A}^a_{j,\varepsilon}\right)^T & \left(\mathbf{A}^b_{j,\varepsilon}\right)^T \end{bmatrix} \begin{bmatrix} \boldsymbol{\varepsilon}^a \\ \boldsymbol{\varepsilon}^b \end{bmatrix}
\end{aligned} \tag{2}$$

$$\mathbf{Q}_j = \begin{bmatrix} \mathbf{e}^j_{\mathrm{n}} & \mathbf{e}^j_{\mathrm{t}} \end{bmatrix}^T,\ \mathbf{A}^i_{j,u} = \begin{bmatrix} \mathbf{Q}_j\mathbf{H}^i_{\mathrm{R}}(\mathbf{r}^i_1) \\ \mathbf{Q}_j\mathbf{H}^i_{\mathrm{R}}(\mathbf{r}^i_2) \end{bmatrix}^T,\ \mathbf{A}^i_{j,\varepsilon} = \begin{bmatrix} \mathbf{Q}_j\mathbf{H}^i_{\mathrm{C}}(\mathbf{r}^i_1) \\ \mathbf{Q}_j\mathbf{H}^i_{\mathrm{C}}(\mathbf{r}^i_2) \end{bmatrix}^T,\ i = a,b \tag{3}$$

$$\mathbf{A}^T_u\mathbf{u} + \mathbf{A}^T_\varepsilon\boldsymbol{\varepsilon} = \mathbf{q} \tag{4}$$

The flow rule for the strain variables is associated with Mohr-Coulomb criterion for the continuum [17]. Given the nonlinearity of the standard Mohr-Coulomb relation (see Eq. (5) and Figure 2a), we follow the solution proposed by Bottero et al. [18] to

implement a linearization (Figure 2b). We use p planes to approximate the real yield relation. The equation of the kth plane is given in Eq. (6), where coefficients A_k, B_k, and C_k are given in Eq. (7).

$$F_{\mathrm{c}}\left(\sigma_x,\sigma_y,\tau_{xy}\right)=\left(\sigma_x-\sigma_y\right)^2+\left(2\tau_{xy}\right)^2-\left(2c\cos\phi-\left(\sigma_x+\sigma_y\right)\sin\phi\right)^2=0 \tag{5}$$

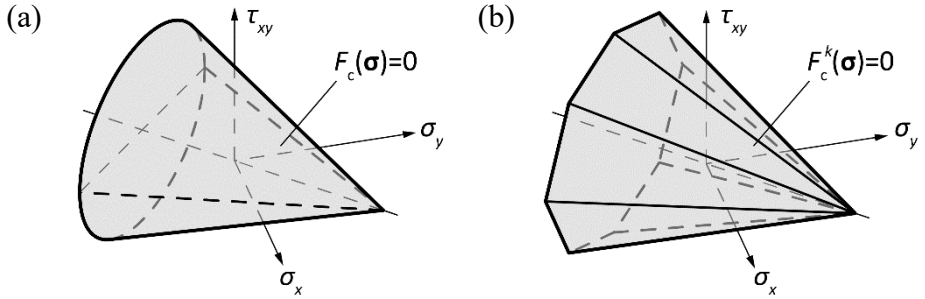

Figure 2: Limit surface of 2D Mohr-Coulomb friction model: (a) original limit surface; (b) linearizing approximation of the limit surface.

$$F_{\mathrm{c}}^k\left(\sigma_x,\sigma_y,\tau_{xy}\right)=A_{\mathrm{c}}^k\sigma_x+B_{\mathrm{c}}^k\sigma_y+C_{\mathrm{c}}^k\tau_{xy}-2c\cos\phi=0 \tag{6}$$

$$\begin{cases} A_{\mathrm{c}}^k=\sin\phi+\cos a_k \\ B_{\mathrm{c}}^k=\sin\phi-\cos a_k \ , \ a_k=2\pi k/p, \ k=1,2,\ldots,p \\ C_{\mathrm{c}}^k=2\sin a_k \end{cases} \tag{7}$$

After the linearization of constitutive relation, the associated flow rule can also be written as a linear constraint (Eq. (8)), where the plastic strain components for each element are linked with p non-negative plastic multipliers.

$$\mathbf{M}^T\dot{\boldsymbol{\lambda}}=\boldsymbol{\varepsilon},\ \dot{\boldsymbol{\lambda}}\geq 0 \tag{8}$$

$$\begin{aligned} \text{minimize} \quad & -\mathbf{f}_D^T\mathbf{u}+\mathbf{c}_0^T\mathbf{p}+\mathbf{c}_1^T\dot{\boldsymbol{\lambda}} \\ \text{subject to} \quad & \mathbf{f}_L^T\mathbf{u}=1 \\ & \mathbf{A}_u^T\mathbf{u}+\mathbf{A}_\varepsilon^T\boldsymbol{\varepsilon}=\mathbf{q} \\ & \mathbf{N}^T\mathbf{p}=\mathbf{q},\mathbf{p}\geq 0 \\ & \mathbf{M}^T\dot{\boldsymbol{\lambda}}=\boldsymbol{\varepsilon},\dot{\boldsymbol{\lambda}}\geq 0 \end{aligned} \tag{9}$$

Now we have all the essential elements for the UB limit analysis, and the optimization formulation for this problem can be stated as Eq. (9). In the objective function, we account for the potential power of the system as well as the dissipation caused at the interfaces and in the elements. The constraint list includes the compatibility condition (4) and flow rule for the elements (8). The interfacial flow rule is associated with the widely acknowledged Mohr-Coulomb friction model [19] (third constraint in the list of Eq. (9)). We also have to supplement a positive work condition to ensure the positive dissipation of the external work [20] (first constraint in Eq. (9)).

2.1 Automatic remeshing procedure

In this subsection, we proceed to construct a proper scheme for the iterative re-meshing procedure based on the above limit analysis formulation (Eq. (9)). As mentioned in the introduction, since the mesh arrangement usually has a considerable influence on the limit analysis prediction, developing a robust remeshing algorithm is necessary to get a result that is less dependent on the mesh.

An automatic remeshing procedure is usually iterative with several analysis steps. In each iteration, we decide on elements that need to be remeshed and then implement the specific refinement schemes to reduce their size. The elements that need to be remeshed are determined according to an energy-based criterion. A dissipation-based indicator γ_{de} is assigned for each element, being defined as the proportion of dissipation of this element and the maximum dissipation over all the elements (Eq. (10)). Therefore, after getting the solution of iteration $k-1$, we compute γ_{de} for each element, and the element whose dissipation index exceeds the threshold γ will be selected as a candidate for further remeshing. Here, as we could expect, the setting of threshold γ is very critical. A smaller choice of γ will lead to more elements being remeshed in one step, and the time consumption of the procedure may become unacceptable. On the contrary, a large threshold may give rise to a low convergence speed.

$$\gamma_{\text{de}} = \left[\frac{\mathbf{c}_{1,1}^T \boldsymbol{\lambda}_1}{P_{\max}} \quad \frac{\mathbf{c}_{1,2}^T \boldsymbol{\lambda}_2}{P_{\max}} \quad \cdots \quad \frac{\mathbf{c}_{1,n}^T \boldsymbol{\lambda}_n}{P_{\max}} \right]^T \tag{10}$$
$$P_{\max} = \max \left\{ \mathbf{c}_{1,i}^T \boldsymbol{\lambda}_{[k-1],i},\ i = 1, 2, \cdots n \right\}$$

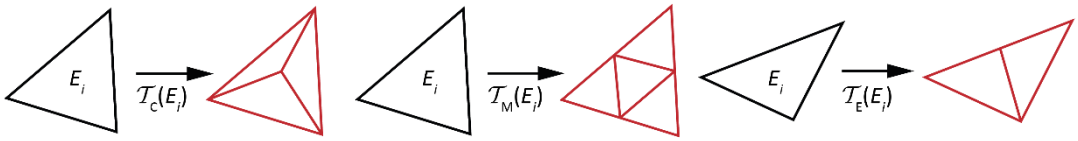

(a) Centroid refinement (b) Mid-point refinement (c) Edge-split method

Figure 3: Refinement scheme for triangle elements.

Regarding the refinement, we propose three different schemes for each selected element candidate. In the centroid scheme (Figure 3a), we added an extra node at the centroid of the triangle, and the origin element is divided into three. The mid-point refinement and the edge-split method are inspired by the remeshing scheme proposed in [14] for the structured mesh. In the mid-point refinement (Figure 3b), mid-point nodes are added to three edges of the triangle to generate four sub-triangles. Note that after such refinement, all these sub-triangles are similar to the original element, and the direction of the new interfaces always remains parallel to the original one. The edge-split refinement is the most simple and direct approach (Figure 3c), where the triangle is split along the linkage of the mid-point of the longest edge and the opposite vertex. In this scheme, the increase of the element amount is the fewest. Associated the refinement scheme with the previous element selection approach, the whole iterative remeshing scheme is clear now (see Algorithm 1). In the below analysis, we will

first present a benchmark example to compare the effectiveness of this procedure with the appliance of these three schemes.

Algorithm 1 Iterative remeshing scheme

1. Solve (9) and Get initial solution $\mathbf{u}_{[0]}$, $\mathbf{p}_{[0]}$, $\boldsymbol{\lambda}_{[0]}$, α_0;
2. Initial setting: $e = 1$, tol=0.001, $k = 0$;
3. **WHILE** $e > tol$
4. $k = k + 1$;
5. Calculate dissipation-based indicator γ_{de} for each element
6. Find the element where the dissipation exceeds the threshold
$$E_{\mathrm{re}} = \left\{ E_i : \gamma_{\mathrm{de},[k\text{-}1]}\left(E_i\right) > \gamma \right\}$$
7. Refine element set E_{re} through refinement scheme $\mathrm{T_C}/\mathrm{T_M}/\mathrm{T_E}$ and get the new model
8. Solve (9) and get the results $\mathbf{u}_{[k]}$, $\mathbf{p}_{[k]}$, $\boldsymbol{\lambda}_{[k]}$, $\alpha_{[k]}$ for the new model
9. Calculate error of the load multiplier $e = |\alpha_{[k]} - \alpha_{[k-1]}|/\alpha_{[k-1]}$
10. **END**

3 Results

In this section, we will present two case studies with the implementation of the proposed automatic remeshing procedure. We first investigate a classic benchmark of geomechanics, the strip footing problem, to compare the performance of different refinement schemes. Then, the approach will be applied to the collapse analysis of Prestwood Bridge, which is a more practical and large-scale scenario.

3.1 Benchmark example: strip footing problem

To test the effectiveness of different refinement schemes for triangles, we first apply the proposed remeshing procedure to the strip footing problem. The case considered here is the collapse of weightless cohesive-frictional soil. The geometry, load and boundary conditions refer to the simulation carried out by Sloan and Kleeman [4] (Figure 4a). The unit length B for the geometry is equal to 1000 mm and the depth of the soil is also 1000 mm. The effective cohesion c and friction angle φ are 1 MPa and 30°, respectively, and the linearization precision p for the Mohr-Coulomb relation is set as 24. We start from the same unstructured triangular mesh (generated by a MATLAB-based code package "MESH2D" [21], Figure 4b) and implement the proposed remeshing procedure with the three refinement schemes proposed above, through which the accuracy and efficiency of these three procedures can be compared. The threshold factor γ for the element selection criterion is set as 0.6. For the standard procedure, the iteration will stop only when the error of the collapse load is reduced to the tolerance. However, it could be quite time-consuming for some of the considered refinement cases. Given the comparative purpose of this benchmark study, for each case, the procedure will stop at the 10th iteration whether the convergence criterion is reached or not, to control the computational budget at an acceptable level.

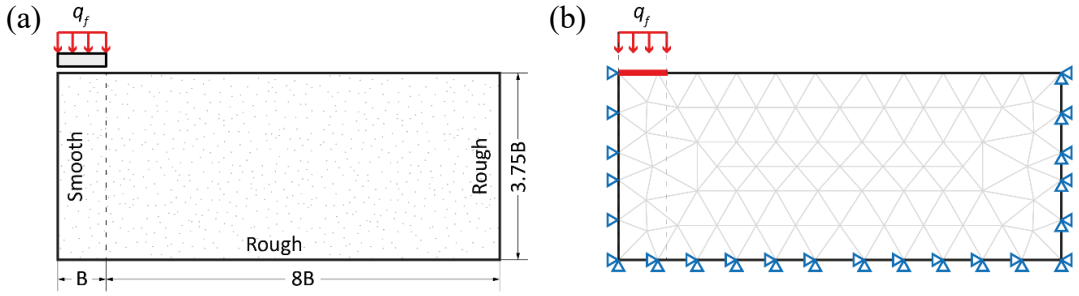

Figure 4: Modeling of strip footing problem [4]: (a) geometry, load and boundary conditions; (b) Initial mesh for the remeshing procedure.

Figure 5 gives the convergence curves of these 10 iterations for different refinement schemes. We can see the proposed procedure is quite effective as the collapse load is continuously reduced due to the iterative refinement, whatever triangular refinements are employed. Nevertheless, the convergence speed and the efficiency of those refinement iterations are different. Note that for this benchmark problem, the analytical solution is available, which is 30.14MPa [4]. We also indicate this benchmark value through a red line in Figure 5.

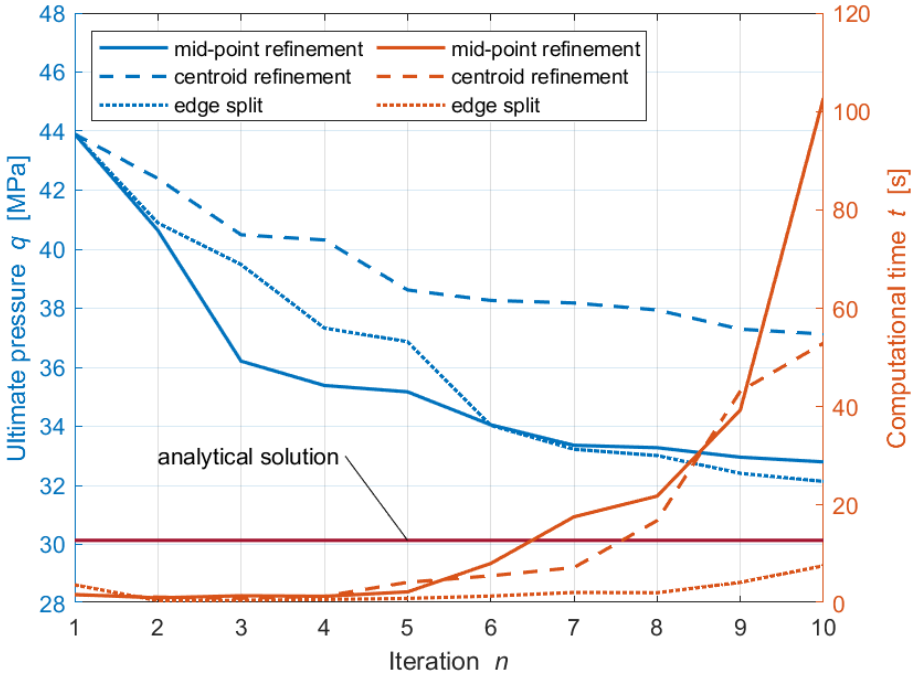

Figure 5: Convergence of the ultimate pressure and growth of the computational time during the remeshing procedure for the strip footing problem: comparison of different triangular refinements.

In fact, the convergence speed of the centroid refinement (Figure 5) is not as rapid as our expectation. Although the collapse load has dropped during the iteration, the final prediction is still quite discrepant from the analytical solution (about 23.2%). This could be attributed to the inefficiency of this refinement scheme itself. As we can

expect, continuous cracking paths are hard to form when iteratively applying this scheme. In the final step of the remeshing, we can note that all the generated cracks are radial from the nodes but not linked with each other to configure a successive path (Figure 6b). In contrast, the performance of the mid-point refinement is very acceptable since all the generated interfaces between the elements are parallel to the original edges. The new cracking configuration excellently inherits from the continuity of the initial mesh (Figure 6c). However, note that the elements near the primary cracks are repeated to be split into a very small size in the later iterations. This gives rise to an explosion of the element amount and further a high time consumption of the analysis: in the final iteration, the time cost for the mid-point refinement can reach twice that of the centroid refinement (see Figure 5). The edge-split method presents the highest computational efficiency, as the new elements generated from this scheme are the fewest (see Figure 5). Moreover, the direction of the interfaces generated by this scheme is much more diverse, while the continuous configuration of those interfaces fairly remains after several iterations. This increases the possibility of the occurrence of different crack patterns. As a result, the final load prediction is also the most conservative among all the three approaches (deviations within 7%).

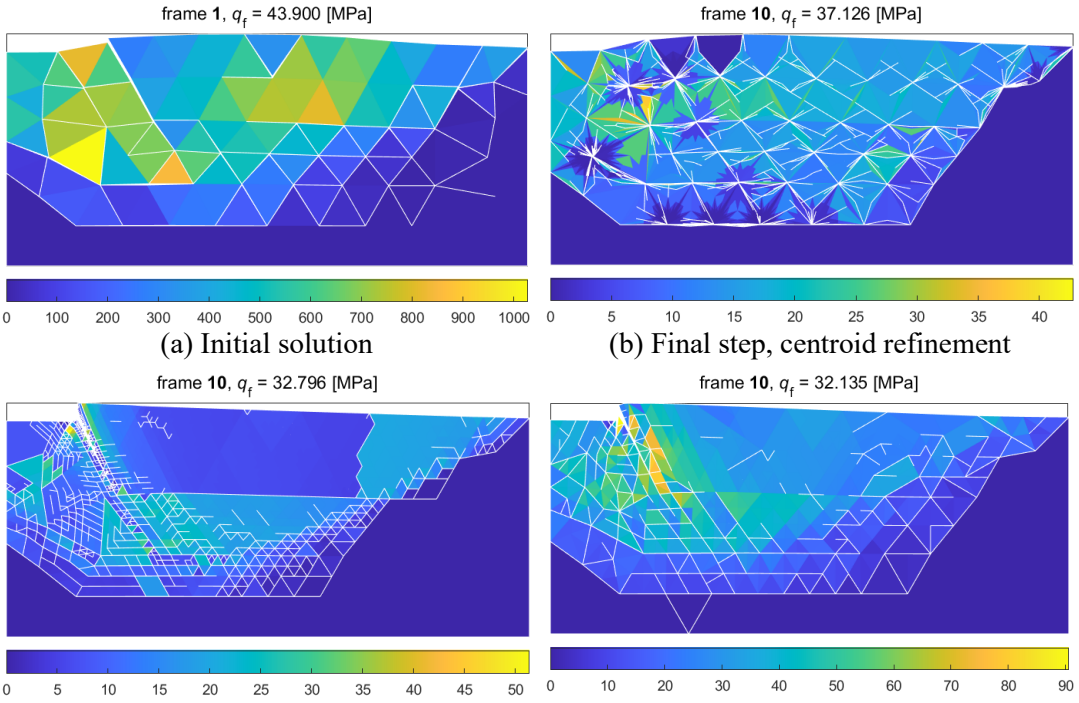

(a) Initial solution (b) Final step, centroid refinement

(c) Final step, mid-point refinement (d) Final step, edge-split method

Figure 6: Collapse of the strip footing problem with the appliance of remeshing procedure: comparison of different refinement schemes, element dissipation.

Table 1 collects the predicted results and the computational cost for the remeshing procedure with all three refinement schemes. We see convergence speed for the mid-point refinement and edge-split approaches are prominent. The drop of the load prediction after 10 refinement iterations can reach 25%. These two approaches also give a more accurate estimation of the collapse load in the final step. The deviation from

the precise analytical solution is 6.6 – 8.7%. As we mentioned above, the edge-split scheme also presents remarkable efficiency. The element amount used in the final step is the fewest and the computational consumption is 8 – 15% of the other two refinement schemes. Therefore, according to this benchmark study, we can conclude that the edge-split method is the best refinement scheme for the remeshing procedure. In the below analysis for a more large-scale problem, only the edge-split method will be adopted for the remeshing procedure.

Re-mesh scheme	$q_{f,[1]}$ [MPa]	$q_{f,[end]}$ [MPa]	Drop of load (%)	Computational time t (s)	Analytical solution [MPa]
Centroid refinement		37.126	15.431	52.913	
Mid-point refinement	43.9	32.796	25.294	102.734	30.14
Edge-split method		32.135	26.800	7.661	

Table 1: Summary of the results and computational cost for the three refinement schemes.

3.2 Collapse of Prestwood Bridge

After concluding the most efficient refinement approach, we now apply this remeshing procedure to a more practical scenario, the collapse analysis of a real bridge with full consideration of the backfill. This bridge is also a very classical benchmark since it has been studied by many previous researchers.

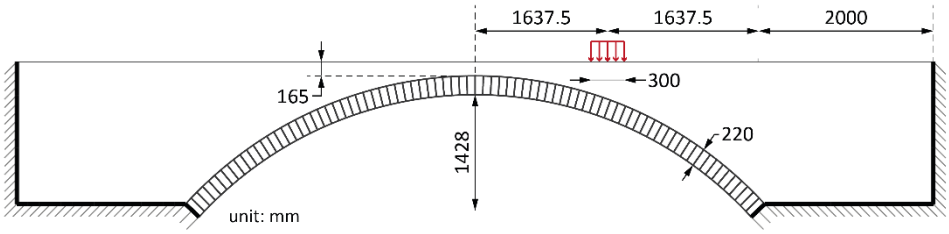

Figure 7: Geometry of Prestwood Bridge [9-10].

The span of the bridge is 6550 mm, with a rise of 1428 mm. The thickness of the arch ring is 220 mm. Detailed geometric characteristic of this bridge is shown in Figure 7 [9-10]. The boundary at the side and bottom of the backfill as well as the springer are all unilateral contact conditions. The load pattern considered here is a pressure with a width of 300 mm, acting at the 1/4 span of the bridge. The 80 bricks of the ring are considered rigid elements, arranged according to the real bond pattern. The backfill region will be discretized by the aforementioned deformable triangular elements, and the proposed remeshing procedure will be employed to refine the elements in this region. Regarding the constitutive model of the backfill, besides the standard Mohr-Coulomb model, we also include the criterion of tension cut-off [9-10] and the corresponding constraint shares the same expression as Eq. (8) after the linearization. Therefore, we can keep solving using Eq. (9) to get the collapse results. The material parameters for the brick, infill, and interfaces are listed in Table 2.

	Elements		Interfaces		
	brick	backfill	Brick-to-brick	Brick-to-backfill	Backfill-to-backfill
Density ρ [kg/m^3]	20	20	-	-	-
Frictional angle φ [°]	-	37	37	37	37
Cohesion c [MPa]	-	0.01	10^{-6}	10^{-6}	0.01
Tensile strength σ_t [MPa]	-	0	0	0	0

Table 2: Material parameters for the elements and interfaces, Prestwood bridge.

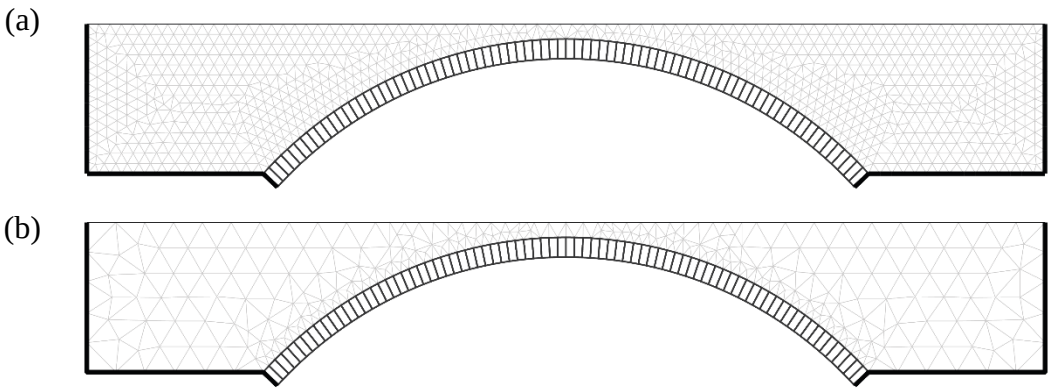

Figure 8: Triangular mesh for the backfill of Prestwood Bridge: (a) fine mesh; (b) initial coarse mesh for the remeshing procedure.

The triangular mesh generator employed here is also "MESH2D" [21]. For a benchmark purpose, we first present the result of the single-step limit analysis through solving (9), without appliance of the remeshing. The mesh size for the backfill region is quite fine. The total amount of triangles for the discretization is 1605 (Figure 10a).

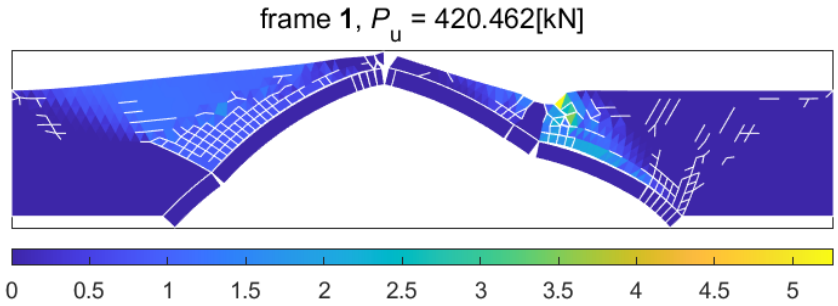

Figure 9: Collapse of Prestwood bridge predicted from the standard limit analysis: dissipation distribution.

In this case, the overall collapse mechanism of the arch is basically the standard 4 hinge mechanism (Figure 9). Instead of the occurrence of a single hinge, however, clusters of hinges appear at the keystone or springer due to the presence of infill, and

the locations agree with the one indicated in the classic 4 hinge mechanism. The loading area of the backfill moves downward due to the pressing, while the left part of the fill side goes up along with the deformation of the ring. The infill elements in these two regions thus present a large dissipation, with rich crack propagations. Short cracks also spread at the backfill near the right springer, due to the appearance of multiple intrados hinges.

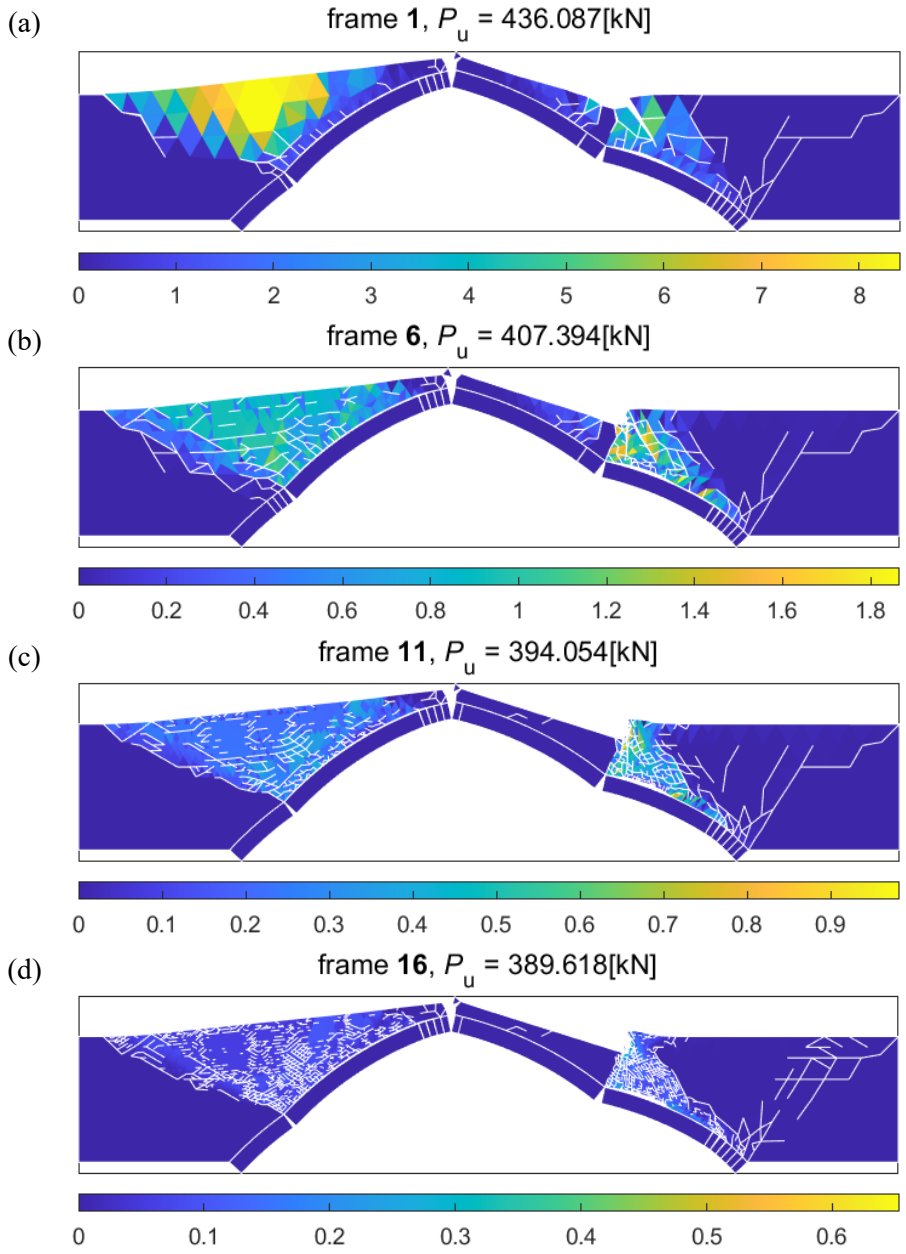

Figure 10: Collapse of Prestwood bridge predicted from the limit analysis with iterative remeshing procedure: dissipation distribution.

Then, we employ the proposed remeshing procedure to analyze the collapse of Prestwood Bridge. Given the best performance of edge-split refinement, below we

only consider this scheme to refine the element candidates in each iteration. The convergence criterion is based on the error of the load prediction, where the tolerance e is set as 0.001. In the initial model, a coarse mesh for the backfill region is employed (see Figure 8b, also generated by "MESH2D" [21]). The amount of the element is 568. Critical frames of the collapse prediction during the iterations are given in Figure 10.

In the initial solution, we can find that the overall motion of the bridge is analogous to the result from the one-step limit analysis, and the distribution of the large-dissipated infill elements is generally the same (see Figure 9). However, the dissipation at the left passive-motion area is significantly higher, while in the loading area at the right, we note a crack with a very broad separation. Both of them are the consequence of employing the element with a large size. Further refinement of the element appears in those infills with large deformation, which rapidly decreases the dissipation in the backfill. In step 6, the collapse load has decreased below the prediction of limit analysis without remeshing. In the final several iterations, the mesh of the infill in the left passive motion and the right external loading areas have become extremely fine. We also note that numerous micro-cracks appear in those two regions, instead of the several large cracks in the initial solution. As a result, the behavior of these two areas of backfill becomes more deformable. The converged load prediction in the last step is 7.4% more conservative than the one from the normal limit analysis. However, we should remark on the explosion of the number of elements due to the successive appliance of the refinement scheme.

4 Conclusions

This paper has developed a remeshing procedure for the finite element limit analysis with unstructured triangular mesh. In each iteration, we select the element candidates with large energy dissipation and then apply the specific scheme to refine these elements. Three different refinement schemes are proposed. To understand their performance, the remeshing procedure implementing those three refinement approaches was first applied to analyze the strip footing problem as a comparative study. Then, the remeshing procedure was employed to refine the mesh of the backfill region when analyzing the collapse of Prestwood Bridge, to test the robustness and efficiency of this approach in more large-scale problems.

The results of the strip footing problem demonstrate the effectiveness of the proposed approach. The load prediction becomes close to the analytical solution after the iterations, whatever refinement approaches are employed. Among all the refinement schemes proposed, the edge-split refinement performs the best in the aspect of both accuracy and efficiency. The deviation of the final prediction is within 7% while the time consumption is 8 – 15% of the other two counterparts. The case study of Prestwood Bridge further illustrates the excellent robustness of the remeshing procedure in a more large-scale scenario, through which the mesh dependence of the results can be effectively reduced. After several iterations, the predicted load has dropped below the estimation from the normal limit analysis with a fine mesh. Moreover, the computational cost of the remeshing procedure at this stage is also comparatively inexpensive.

However, such cost may rapidly grow in the final several iterations before the convergence due to the explosion of the element amounts.

Acknowledgements

Yiwei Hua would like to thank the financial support from China Scholarship Council (CSC) under the grant CSC No. 202108320019.

References

[1] F. Tschuchnigg, H.F. Schweiger, S.W. Sloan, "Slope stability analysis by means of finite element limit analysis and finite element strength reduction techniques. Part II: Back analyses of a case history", Comput. Geotech. 70, 178–189, 2015. https://doi.org/10.1016/j.compgeo.2015.07.019.

[2] Z. Jin, C. Zhang, W. Li, S. Tu, L. Wang, S. Wang, "Stability analysis for excavation in frictional soils based on upper bound method", Comput. Geotech. 165, 2024. https://doi.org/10.1016/j.compgeo.2023.105916.

[3] K. Krabbenhøft, A. V. Lyamin, S.W. Sloan, "Three-dimensional Mohr-Coulomb limit analysis using semidefinite programming", Commun. Numer. Methods Eng. 24, 1107–1119, 2008. https://doi.org/10.1002/cnm.1018.

[4] S.W. Sloan, P.W. Kleeman, "Upper bound limit analysis using discontinuous velocity fields", Comput. Methods Appl. Mech. Eng. 127, 293–314, 1995. https://doi.org/10.1016/0045-7825(95)00868-1.

[5] S.W. Sloan, "Geotechnical stability analysis", Geotechnique. 63, 531–572, 2013. https://doi.org/10.1680/geot.12.RL.001.

[6] M. Gilbert, C.C. Smith, I.W. Haslam, T.J. Pritchard, "Application of Discontinuity Layout Optimization to geotechnical limit analysis problems", Numer. Methods Geotech. Eng. - Proc. 7th Eur. Conf. Numer. Methods Geotech. Eng. p. 169–174, 2010.

[7] M. Gilbert, D. Nguyen, C. Smith, "Computational limit analysis of soil-arch interaction in masonry arch bridges", Proc. 5th Int. Conf. Arch Bridg. ARCH. p. 633–640, 2007. http://www.civil.uminho.pt/masonry/Publications/ARCH07/647_654.pdf.

[8] G. Milani, P.B. Lourenço, "3D non-linear behavior of masonry arch bridges", Comput. Struct. 110–111, 133–150, 2012. https://doi.org/10.1016/j.compstruc.2012.07.008.

[9] A. Cavicchi, L. Gambarotta, "Two-dimensional finite element upper bound limit analysis of masonry bridges", Comput. Struct. 84, 2316–2328, 2006. https://doi.org/10.1016/j.compstruc.2006.08.048.

[10] A. Cavicchi, L. Gambarotta, "Collapse analysis of masonry bridges taking into account arch-fill interaction", Eng. Struct. 27, 605–615, 2005. https://doi.org/10.1016/j.engstruct.2004.12.002.

[11] J. Peraire, M. Vahdati, K. Morgan, O.C. Zienkiewicz, “Adaptive remeshing for compressible flow computations”, J. Comput. Phys. 72, 449–466, 1987. https://doi.org/10.1016/0021-9991(87)90093-3.

[12] N.E. Wiberg, X.D. Li, F. Abdulwahab, “Adaptive finite element procedures in elasticity and plasticity”, Eng. Comput. 12, 120–141, 1996. https://doi.org/10.1007/BF01299397.

[13] A. V. Lyamin, S.W. Sloan, “Mesh generation for lower bound limit analysis”, Adv. Eng. Softw. 34, 321–338, 2003. https://doi.org/10.1016/S0965-9978(03)00032-2.

[14] E. Christiansen, O.S. Pedersen, “Automatic mesh refinement in limit analysis”, Int. J. Numer. Methods Eng. 50, 1331–1346, 2001. https://doi.org/10.1002/1097-0207(20010228)50:6<1331::AID-NME46>3.0.CO;2-S.

[15] A. V. Lyamin, S.W. Sloan, K. Krabbenhøft, M. Hjiaj, “Lower bound limit analysis with adaptive remeshing”, Int. J. Numer. Methods Eng. 63, 1961–1974, 2005. https://doi.org/10.1002/nme.1352.

[16] L. Borges, N. Zouain, C. Costa, R. Feijóo, “Adaptive approach to limit analysis”, Int. J. Solids Struct. 38, 1707–1720, 2001. https://doi.org/10.1016/S0020-7683(00)00131-1.

[17] D.C. Drucker, “Coulomb Friction, Plasticity, and Limit Loads”, J. Appl. Mech. 21, 71–74, 1954. https://doi.org/10.1115/1.4010821.

[18] A. Bottero, R. Negre, J. Pastor, S. Turgeman, “Finite element method and limit analysis theory for soil mechanics problems”, Comput. Methods Appl. Mech. Eng. 22, 131–149, 1980. https://doi.org/10.1016/0045-7825(80)90055-9.

[19] M.C. Ferris, F. Tin-Loi, “Limit analysis of frictional block assemblies as a mathematical program with complementarity constraints”, Int. J. Mech. Sci. 43, 209–224, 2001. https://doi.org/10.1016/S0020-7403(99)00111-3.

[20] G. Maier, A. Nappi, “A theory of no-tension discretized structural systems”, Eng. Struct. 12, 227–234, 1990. https://doi.org/10.1016/0141-0296(90)90021-J.

[21] D. Engwirda, “Locally-optimal Delaunay-refinement and optimisation-based mesh generation”, PhD Thesis, The University of Sydney, 2014.